Earth and Planetary Science Letters 473 (2017) 177–189

Contents lists available at ScienceDirect

Earth and Planetary Science Letters

www.elsevier.com/locate/epsl

A 17,000 yr paleomagnetic secular variation record from the southeast Alaskan margin: Regional and global correlations

M.H. Walczak [a,c,*], J.S. Stoner [a], A.C. Mix [a], J. Jaeger [b], G.P. Rosen [b], J.E.T. Channell [b], D. Heslop [c], C. Xuan [a,d]

[a] College of Earth, Ocean, and Atmospheric Sciences, Oregon State University, Corvallis, OR 97331, United States
[b] Department of Geological Sciences, University of Florida, Gainesville, FL 32611, United States
[c] Research School of Earth Sciences, Australian National University, Canberra, ACT, 2601, Australia
[d] School of Ocean and Earth Science, National Oceanography Centre Southampton, University of Southampton, Southampton, SO14 3ZH, UK

ARTICLE INFO

Article history:
Received 15 May 2016
Received in revised form 12 April 2017
Accepted 16 May 2017
Available online 26 June 2017
Editor: B. Buffett

Keywords:
paleomagnetic secular variation
North Pacific
Alaska
Holocene
geomagnetism

ABSTRACT

High-resolution sedimentary records on two cores from the Gulf of Alaska margin allow development of a ~17,400-yr reconstruction of paleomagnetic secular variation (PSV). General agreement between the two records on their independent chronologies confirms that local PSV is recorded, demonstrating that such archives, notwithstanding complexities due to variable sedimentary regimes, deposition rates, and diagenetic conditions, provide meaningful information on past changes of the geomagnetic field. Comparisons with other independently dated sedimentary paleomagnetic records from the NE Pacific indicate largely coherent inclination records that in combination create a NE Pacific sedimentary inclination anomaly stack (NEPSIAS) capturing the common signal over an area spanning >30° longitude and latitude from Alaska through Oregon to Hawaii. Comparisons of NEPSIAS with high quality declination records from the northern North Atlantic (NNA) show that negative (shallow) inclination anomalies in NEPSIAS are associated with eastward NNA declinations while positive (steep) inclination anomalies in NEPSIAS are associated with westward NNA declinations. Comparison of these directional records to regional geomagnetic intensities over the past ~3000 yrs in North America and back nearly 8000 yrs in the Euro/Mediterranean region, are consistent with a driving mechanism of oscillations in the relative strength of the North American and Euro/Mediterranean flux lobes. The persistence of these dynamics through the Holocene implicates a long-lived organizing structure likely imposed on the geomagnetic field by the lower mantle and/or inner core. These observations underscore a fundamental connection between directional PSV in the North Pacific with that of the North Atlantic, supporting the potential for long-distance correlation of directional PSV as a chronostratigraphic tool.

1. Introduction

1.1. Paleomagnetic secular variation

Averaged over tens of thousands of years, Earth's magnetic field can be approximated by a geocentric axial dipole (GAD) (Merrill et al., 1996). However, at any given moment the geomagnetic field expressed at Earth's surface deviates substantially from this idealized morphology (Jackson et al., 2000). Field morphology changes with time, displaying variable tilt of the best-fitting dipole relative to Earth's axis of rotation, as well as non-dipole structures (Merrill et al., 1996). Incomplete understanding of what drives deviation from a GAD, in conjunction with the unresolved temporal and spatial scales over which non-dipolar structures persist (Bloxham and Gubbins, 1987) precludes accurate prediction of future geomagnetic field behavior and hinders our ability to reconstruct past field morphologies. Historical reconstructions indicate the existence of persistent concentrations of geomagnetic flux, such as the Canadian and Siberian flux lobes, which may result from organizing structure imposed on the geomagnetic field by lower mantle heterogeneity (Bloxham and Gubbins, 1987). Patterns of paleomagnetic secular variation (PSV) are unlikely to be random, and the interplay of dipolar and non-dipolar components of the field may allow us to understand the dynamics of geomagnetic change.

Observation-based reconstructions of the global geomagnetic field (Constable et al., 2016; Nilsson et al., 2010, 2011, 2014), as well as dynamo modeling studies (Amit et al., 2011) sug-

* Corresponding author at: College of Earth, Ocean, and Atmospheric Sciences, Oregon State University, Corvallis, OR 97331, United States.
E-mail address: mwalczak@ceoas.oregonstate.edu (M.H. Walczak).

http://dx.doi.org/10.1016/j.epsl.2017.05.022
0012-821X/

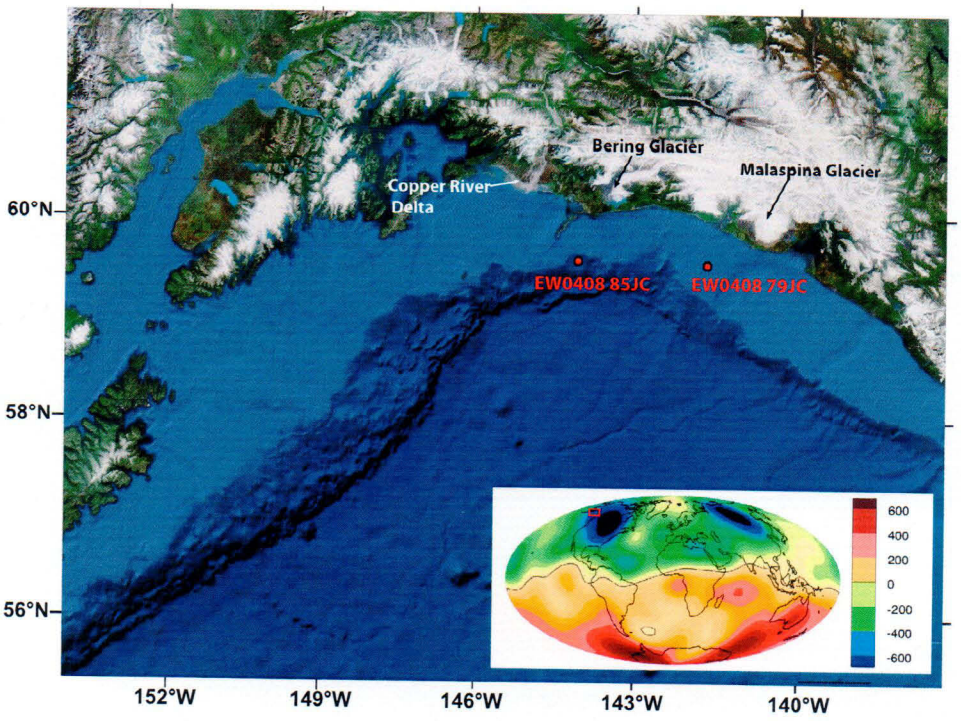

Fig. 1. Site map showing the bathymetry of the Gulf of Alaska, as well as the locations of shelf core EW0408-79JC and slope core EW0408-85JC. The locations of the major sediment sources to the margin, which include drainages from the Bering and Malaspina glaciers as well as the Copper River, are labeled. Inset map (modified from Constable et al., 2016) shows the historical time averaged (1590–1990 C.E) vertical component of the magnetic field at the core/mantle boundary (Jackson et al., 2000); the position of the Gulf of Alaska on the western edge of the North American flux lobe is outlined in red. (For interpretation of the references to color in this figure, the reader is referred to the web version of this article.)

gest that oscillations of flux concentrations at a few recurrent locations could be drivers of mid-latitude PSV. However, alternative conceptual drivers of centennial-to millennial-scale PSV variability, including drift of non-dipole field sources, remain plausible (Nilsson et al., 2010, 2014). Beyond the last 5000 yrs, high-quality observations of PSV behavior are concentrated in the Atlantic sector of the northern hemisphere (Constable et al., 2016; Stoner et al., 2013), while those from the Pacific sector (Verosub et al., 1986; Peng and King, 1992; Geiss and Banerjee, 2003; Lisé-Pronovost et al., 2009) remain rare and have limited temporal resolution and/or chronological control. More detailed records, extending further back in time and covering a larger geographic range, are needed to facilitate a better understanding of the spatial dynamics of the geomagnetic field.

Continental margin sediments can provide greatly expanded, and in many cases well-dated, paleomagnetic records from widely distributed locations. However, interpretations of these records are complicated by variable sedimentation rates, lithogenic sources, transport mechanisms, and diagenetic conditions. Here we reconstruct PSV from the continental margin of the Gulf of Alaska using jumbo piston cores, as well as their attendant trigger (gravity) cores and multi-cores designed to preserve the sediment/water interface; all were collected during R/V Ewing cruise EW0408 in 2004 (Fig. 1). Independent marine radiocarbon chronologies and lithologic variability assessed through computerized tomographic (CT) scans support development of continuous high resolution PSV records that span ~6200 cal ybp on the open continental shelf (Site EW0408-79JC; 59.53°N, 141.76°W, 158 m water depth) and ~17,000 cal ybp from a small depositional basin on adjacent Kayak slope (Site EW0408-85JC; 59.56°N, 144.15°W, 682 m water depth). Comparisons with other independently dated PSV records allow us to evaluate coherence throughout the NE Pacific as well as the relationship of NE Pacific PSV to records from the North Atlantic, Europe, and global field reconstructions.

1.2. Geologic setting: the Gulf of Alaska

The Gulf of Alaska is a tectonically active, glaciated margin. Sedimentation is overwhelmingly terrigenous, with major sources including the drainages of the Bering and Malaspina Glaciers, as well as the Copper River (Fig. 1). Modern accumulation rates on the shelf range from ~0.1–3 cm/yr (Jaeger and Nittrouer, 2006), and expanded lithogenic depositional sequences potentially allow for PSV reconstructions at a resolution impossible to capture in slowly-accumulating deep-sea sediments.

Although there is an opportunity to record the geomagnetic field at high-resolution, marine continental margin records are prone to a variety of complications. The sediment supply to the northeast Gulf of Alaska is diverse, associated with both the proximal erosion of the St. Elias Range by the Bering and Malaspina glaciers, as well as potential distal delivery from the Copper River catchment; these source diverse lithologies that differ in magnetic properties (Cowan et al., 2006), potentially complicating interpretations of normalized remanence. Additionally, while benthic oxygen levels on the margin have been increasing through the Holocene, the early Holocene and late deglacial intervals experienced episodes of benthic hypoxia (Davies et al., 2011; Addison et al., 2012). This can lead to degradation of paleomagnetic records via destruction of primary iron-bearing magnetic remanence carriers during bacterially-mediated anaerobic sulfate reduction (Karlin and Levi, 1983; Tarduno and Wilkinson, 1996), and/or production of secondary magnetic minerals (Roberts et al., 2012).

2. Methods

2.1. Bulk sediment properties

Magnetic susceptibility (MS) and gamma-ray attenuation (GRA) bulk-density data were measured shipboard on whole cores on a

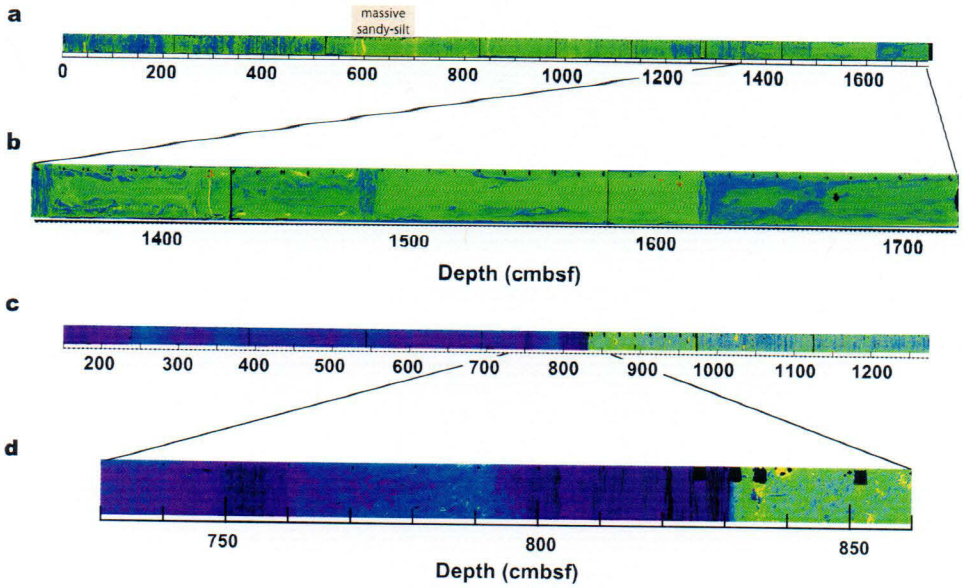

Fig. 2. a) Computerized tomographic (CT) scan of EW0408-79JC, shown in false color to highlight density changes. Warmer (green, yellow) colors indicate high densities associated with coarser lithofacies, while cooler (blue, purple) colors indicate lower densities associated with finer facies and biogenic sedimentation. The massive sandy-silt deposit excluded from paleomagnetic interpretation (575–705 cmbsf) is indicated in orange. **b)** The section below 1350 cmbsf in the core shows vertical flow structures meters in scale, indicative of extreme coring deformation. **c)** Computerized tomographic (CT) scan of EW0408-85JC, shown in false color to highlight density changes (Davies et al., 2011). Warmer (green, yellow) colors indicate high densities associated with coarser lithofacies, while cooler (blue, purple) colors indicate lower densities associated with finer facies and biogenic sedimentation. **d)** The deglacial transition is characterized by abrupt shifts in lithology, as well as intermittent laminae preservation associated with high organic carbon content and low bottom water oxygen content. (For interpretation of the colors in this figure, the reader is referred to the web version of this article.)

GEOTEK MSCL-S multi-sensor core logger at 1 cm intervals. Magnetic susceptibility was measured at 0.5 cm intervals in the split multi-core, trigger-core, and uppermost sections of jumbo piston cores EW0408-85JC using a Bartington MS2E core-logging point sensor (Fig. S.1).

2.2. Computerized tomographic (CT) scanning

Computerized tomographic (CT) density measurements were performed at the Oregon State University College of Veterinary Medicine using a Toshiba Aquilion 64 Slice instrument. Scan collection and processing were conducted following methods in Davies et al. (2011) (Fig. 2).

2.3. Radiocarbon dating

Planktonic foraminifera were picked from the >150 μm grain-size sediment fraction. The two predominant planktonic species for the sites, *N. pachyderma* (sinistral) and *G. bulloides*, were analyzed separately at 604 centimeters below sea floor (cmbsf) in core EW0408-79JC, and at 555 cmbsf in core EW0408-85JC. The resultant *N. pachyderma* radiocarbon age is 10 ± 50 yrs younger than that for the *G. bulloides* in core EW0408-79JC, and 65 ± 50 yrs greater than that for the *G. bulloides* in core EW0408-85JC (Davies et al., 2011). As these differences approximate the measurement uncertainty for the individual samples, for all other depths species were combined to increase sample size and reduce analytical error.

Radiocarbon analyses were performed at the UC Irvine Keck AMS facility. A total of 38 radiocarbon measurements were performed for 37 stratigraphic horizons in core EW0408-85JC: 3 planktonic samples from the trigger core, and 35 planktonic samples from the jumbo piston core (Table A.1; Davies-Walczak et al., 2014). A total of 11 radiocarbon measurements were performed for 10 stratigraphic horizons in core EW0408-79JC (Table A.1). The raw radiocarbon dates were converted to a calendar age scale using the Marine13 calibration (Reimer et al., 2013). To account for regional surface-water reservoir ages of 880 ± 80 yrs, a constant ΔR of 470 ± 80 yrs was applied to all planktonic foraminiferal dates (Davies-Walczak et al., 2014). Correlation of marine tephra layers that have also been dated on land suggest that near-surface marine reservoir ages in this region may vary by at most a few hundred years (Praetorius et al., 2016). To generate age-depth relationships for the cores, we apply a Bayesian probabilistic model (BChron; Haslett and Parnell, 2008) to the remaining calibrated planktonic foraminiferal dates, assuming constant reservoir ages with respect to a changing atmosphere (Davies-Walczak et al., 2014).

2.4. Magnetic methods

Natural remanent magnetization (NRM) of u-channel samples was measured using a 2G Enterprises cryogenic magnetometer at the University of Florida. NRM measurements were performed at 1-cm spacing, though each data point reflects an integral within the magnetometer's pickup coils detection window, which resembles a Gaussian response function (~4.5 cm width at half height). Measurements were made before demagnetization and after 14 alternating-field (AF) demagnetization steps with peak AF from 10–100 mT at 5 mT increments between 10–50 mT and 10 mT increments between 50–100 mT.

Low-field volumetric magnetic susceptibility (κ) measurements of u-channel samples were performed at 1-cm spacing at the University of Florida using a Saffire Instruments SI2B magnetic susceptibility loop system. Anhysteretic remanent magnetization (ARM), also expressed as anhysteretic susceptibility of ARM (κ_{ARM}), was applied to each u-channel in a peak AF of 100 mT, with a 50 μT direct current (DC) bias field, and measured at 1-cm intervals prior to and after AF demagnetization at the same steps used for NRM up to 80 mT. Isothermal remanent magnetizations (IRM) were produced using pulsed DC fields of 0.3 T ($IRM_{0.3T}$) and 0.95 T ($IRM_{0.95T}$, assumed to represent a saturating field and generate a saturation isothermal remanent magnetization, SIRM) applied down the $+Z$ axis and a reversed DC field of 0.3 T applied

down the $-Z$ axis ($IRM_{-0.3T}$). The $IRM_{0.3T}$ was measured prior to and after demagnetization at the same steps used for ARM, while the $IRM_{0.95T}$ and $IRM_{-0.3T}$ were measured prior to and after AF demagnetization at peak fields of 30 and 60 mT. To evaluate coercivity and magnetic mineralogy, S-ratios were calculated according to Bloemendal et al. (1992), via normalization of the $IRM_{-0.3T}$ by the $IRM_{0.95T}$. Values approaching 1 indicate a lower coercivity ferrimagnetic mineralogy (e.g. magnetite), while lower values indicate higher coercivities and a potential antiferromagnetic mineralogic (e.g. hematite) contribution.

To better evaluate potential variability of magnetic remanence carriers through the lithologic units of EW0408-85TC/JC, hysteresis, backfield, IRM thermal demagnetization, and room temperature to low-temperature SIRM (RTLTSIRM) experiments were performed on nine samples from the late Holocene, early Holocene/deglacial transition, and late glacial portions of the core at the Institute for Rock Magnetism at the University of Minnesota. Hysteresis parameters including saturation remanence (M_{rs}), saturation magnetization (M_s), coercivity (B_c), and coercivity of remanence (B_{cr}) were acquired and IRM was imparted for thermal demagnetization measurements in a field of 1 T on a Princeton Measurements Corporation MicroMag vibrating sample magnetometer (VSM). A 2.5 T SIRM was acquired and measured while cooling from 300 K to 10 K and then warming back to 300 K (RTLTSIRM) on a Quantum Design Magnetic Properties Measurement System. Additional hysteresis and backfield measurements were made using a VSM at the Pacific NW Paleomagnetism Laboratory at Western Washington University.

3. Results

3.1. Generation of composite depth scale

Composite sediment depths in centimeters-below-sea-floor (cmbsf) were established empirically using visual correlation of point-source magnetic susceptibility and gamma density data to align the jumbo piston cores with their trigger cores and attendant multi-cores (Fig. S.1). At the site of core EW0408-79JC, the jumbo piston core did not detectably lose sediment at the core top. Trigger core EW0408-79TC apparently lost 13 cm of core top, while multi-core EW0408-78MC7 captured the sediment/water interface. The resultant cmbsf scale for site EW0408-79JC therefore adds 13 cm to the measured trigger core depths. At the site of core EW0408-85JC, the jumbo piston core lost 150 cm of core top. Trigger core EW0408-85TC lost 13 cm of core top, while the multicore EW0408-84MC8 successfully captured the sediment/water interface. Therefore, to generate a composite cmbsf scale for site EW0408-85JC, 150 cm were added to the measured jumbo core depths and 13 cm were added to the measured trigger core depths (Davies et al., 2011).

3.2. Chronology

Assuming constant accumulation rates below the deepest dated interval (1204 cmbsf), the portion of shelf core EW0408-79JC not disturbed by coring (0 to 1350 cmbsf) extends to 6260 cal ybp (Fig. 3). Accumulation rates range from ~100 to 800 cm/kyr in the jumbo piston core, with highest sedimentation rates in the upper 600 cmbsf (~1500 cal ybp), peaking in the 200 to 500 cmbsf interval (~800 to 1000 cal ybp). Slope core EW0408-85JC spans 17,400 cal ybp (Fig. 3), and documents the most recent deglaciation of the NE Pacific (Davies et al., 2011). Accumulation rates range from ~10 cm/kyr during two laminated intervals following regional ice retreat in the Bølling and post-Younger Dryas, to >500 cm/kyr during ice-proximal marine sedimentation in the lower 440 cm of the core.

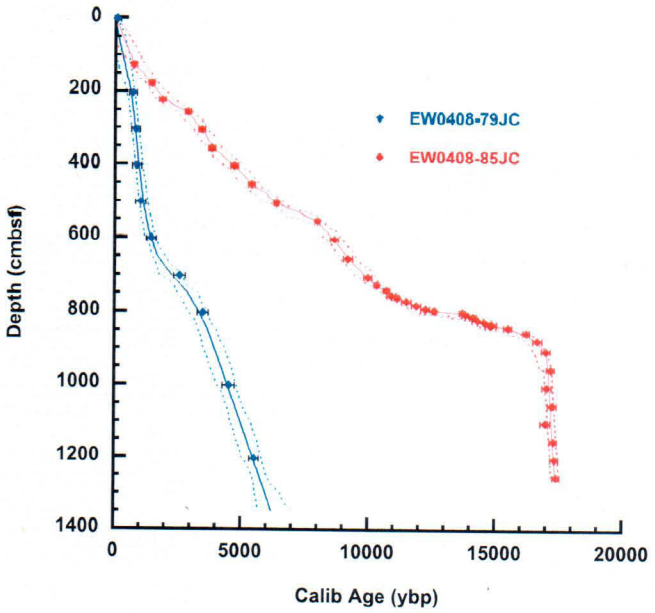

Fig. 3. Calibrated planktonic foraminiferal radiocarbon dates used to generate the age models for EW0408-79JC (blue diamonds) and EW0408-85JC (red diamonds; Davies-Walczak et al., 2014). Depth, on the vertical axis, is plotted on a composite centimeters-below-seafloor (cmbsf) scale described in methods and illustrated in supplemental figure S.1. Dates were converted to calendar ages using the Marine13 calibration and ΔR of 470 ± 80 yrs (see text for details). Plotted error bars on individual dates and the error windows of the age models represent ± 1-σ uncertainty. The solid lines reflect the weighted mean age, while the dashed lines represent the upper and lower 1-σ uncertainty limits of the age-depth model. (For interpretation of the references to color in this figure, the reader is referred to the web version of this article.)

3.3. Lithology

The shelf core EW0408-79JC comprises mainly dark greenish-gray bioturbated silty clay, with interbedded sand/silt layers ranging from sub-millimeter to several centimeters in thickness. The CT-scan imagery shows strong vertical deformation structures in the sediment recovered below 1350 cmbsf (Fig. 2b), reflecting a complete distortion of primary depositional fabric and as such was excluded from interpretation.

The CT scan imagery, supported by the core logger (MSCL) data and radiocarbon dates, suggest that core EW0408-79JC can be crudely divided into two distinct depositional units (Fig. 2). The interval from 0 to 550 cmbsf display well-preserved (450–400 cmbsf) to partially-bioturbated laminations and bi-modal densities averaging $\sim 1.79 \pm 0.1$ g/cm^3, contrasting with a more homogeneous unit between ~550–1200 cmbsf characterized by overall higher density ($\sim 1.82 \pm 0.04$ g/cm^3) and punctuated by occasional sandy layers with sharp and sometimes erosive basal contacts. At depths of ~1200–1350 cmbsf, CT scans suggest a similar lithofacies to the uppermost portion of the core, with strong density contrasts and partially-bioturbated laminations (Fig. 2). The preservation of laminations on the oxygenated shelf suggests that episodic sedimentation rates exceed 2 cm/yr (Jaeger and Nittrouer, 2006) in those intervals.

The homogeneous sandier unit in core EW0408-79JC between ~550–1200 cmbsf is capped at 575–705 cmbsf by a massive sandy-silt layer with anomalously high κ and a sharp basal contact (Figs. 2 and 4). This massive unit has a magnetic and bulk lithology distinct from the overlying and underlying sediments and may have been deposited nearly instantaneously. As a result we exclude these depths from paleomagnetic interpretation (Fig. 4).

Slope core EW0408-85JC captures distinct changes in lithology that reflect the environmental history of the Gulf of Alaska

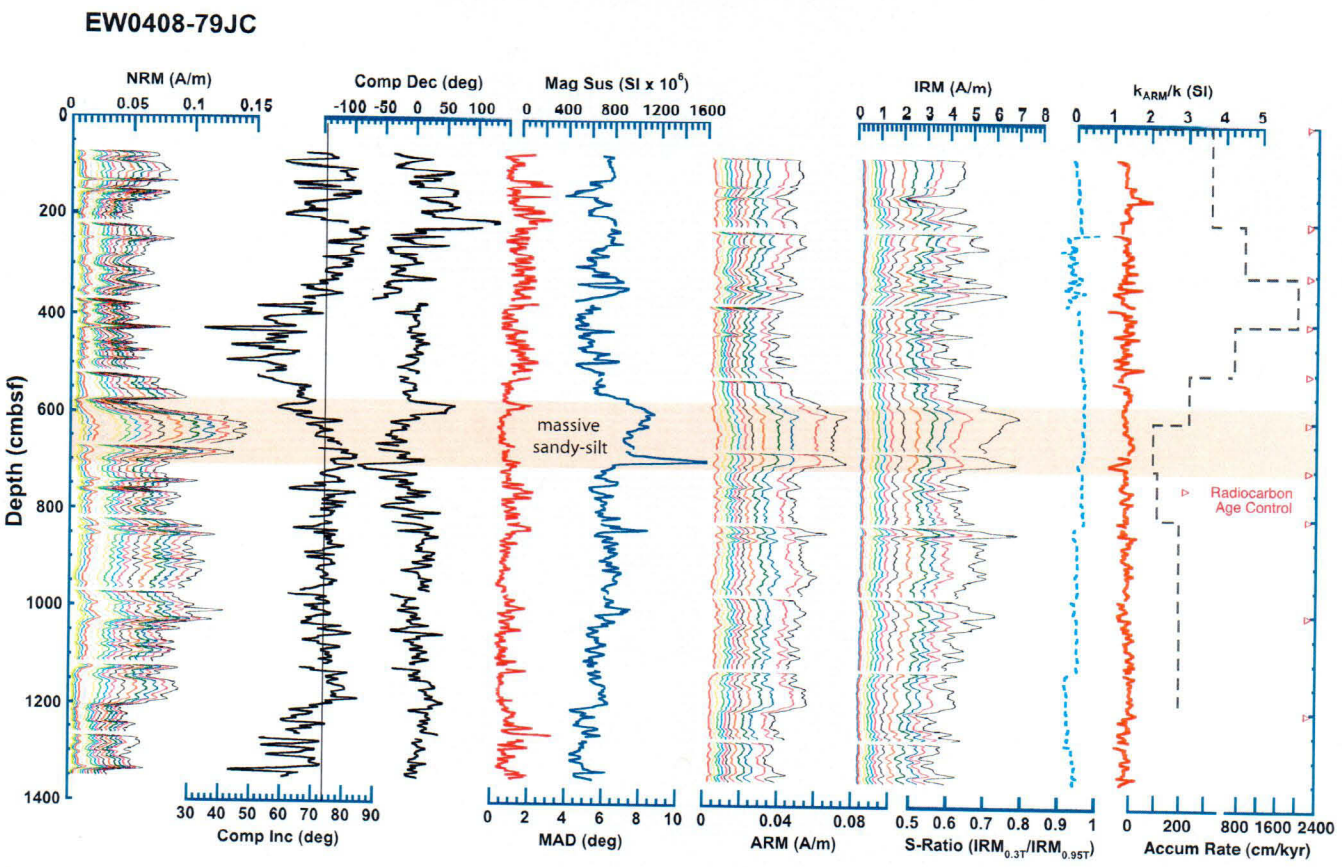

Fig. 4. Bulk magnetic parameters from EW0408-79JC. From left to right: natural remanent magnetization (NRM) intensities after AF-demagnetization at steps from 0–100 mT, component inclinations (GAD = 74°, shown as dashed line), declinations, and maximum angular deviations (MAD) calculated from the 10–60 mT steps, magnetic susceptibility, anhysteretic remanent magnetization (ARM) and isothermal remanent magnetization (IRM) acquired at a 0.3 T DC field after AF-demagnetization at steps from 0–80 mT, S-Ratio, κ_{ARM}/κ, and sediment accumulation rates derived from the planktonic radiocarbon dates (red triangles). The massive sandy-silt deposit excluded from paleomagnetic interpretation (575–705 cmbsf) is indicated in orange. (For interpretation of the colors in this figure, the reader is referred to the web version of this article.)

over the last 17,400 yrs, including the retreat of the Cordilleran ice sheet in the late Pleistocene and large-scale oceanographic changes during the transition into relatively stable Holocene climate conditions (Fig. 2) (Davies et al., 2011). The deepest unit, from the base of the core at ~1270 cmbsf to 831 cmbsf, consists of a massive dark gray diamict interpreted as reflecting ice-proximal glacial-marine sedimentation (Davies et al., 2011). At 831 cmbsf there is a sharp contact with a relatively low-density laminated unit 34 cm thick (Fig. 2d), reflecting high primary productivity and low bottom-water oxygen content, an interpretation supported by excess concentrations of Mo and U (Davies et al., 2011; Addison et al., 2012). There is an increase in lithogenic sediment with coarse pebbles interpreted as ice-rafted debris between 745 and 797 cmbsf (Fig. 2b). This unit reflects a return to glacial conditions accompanying a decrease in primary productivity and renewed bottom-water oxygen (Davies et al., 2011; Addison et al., 2012). From 0–745 cmbsf, sedimentation at the site is broadly characterized by bioturbated dark-gray silty clays, although the interval from 730–745 cmbsf is weakly laminated and has elevated Mo and U contents, indicating a second episode of low bottom-water oxygen in the early Holocene (Davies et al., 2011; Addison et al., 2012).

3.4. Natural and laboratory remanent magnetizations

Component magnetic directions (declination and inclination) and their maximum angular deviations (MAD) were calculated using the principal component analysis method on all steps from 10–60 mT (Kirschvink, 1980), establishing the characteristic remanent magnetization (ChRM). Figs. 4 and 5 show the NRM intensities, ChRM directions and their associated MAD values, magnetic susceptibility, ARM and IRM intensities, S-ratios, κ_{ARM}/κ, and sedimentation rates for jumbo piston cores EW0408-79JC and EW0408-85JC (Figs. S.2 and S.3 present the same data for associated multi- and trigger cores). To better evaluate the interval of low-intensity magnetization sensitive to measurement noise in EW0408-85JC, alternative optimized component directions were also calculated using the 7 most consistent directions from the 14 AF demagnetization steps from 0–100 mT (Figs. S.4 and S.5). Due to lack of azimuthal orientation, declinations are initially rotated to a core mean of zero. ChRM inclinations from both cores are close to their GAD expected values (~74°), and NRM vector components proceed towards the origin with progressive demagnetization (Fig. S.5), suggesting that the geomagnetic field is being recorded with directional fidelity.

For EW0408-79JC, MAD values are generally less than 2° throughout the core, indicating consistently well-defined magnetizations. However, centimeter-scale variations in directions, intensity, and MAD values occur in sediments with partially- to well-preserved primary depositional structures from 0–500 cmbsf (<1100 cal ybp) and at depths greater than 1200 cmbsf (>5500 cal ybp), suggesting that the fine-scale magnetic variations result from this heterogeneous lithofacies. NRM, ARM and IRM intensities (respectively averaging 0.041 ± 0.013 A/m, 0.023 ± 0.004 A/m and 1.61 ± 0.22 A/m after 30 mT AF demagnetization) are consistently higher than those observed in slope core EW0408-85JC. Down-core trends are minimal, although increases in NRM, ARM, and IRM intensities are observed in the higher-density depositional unit

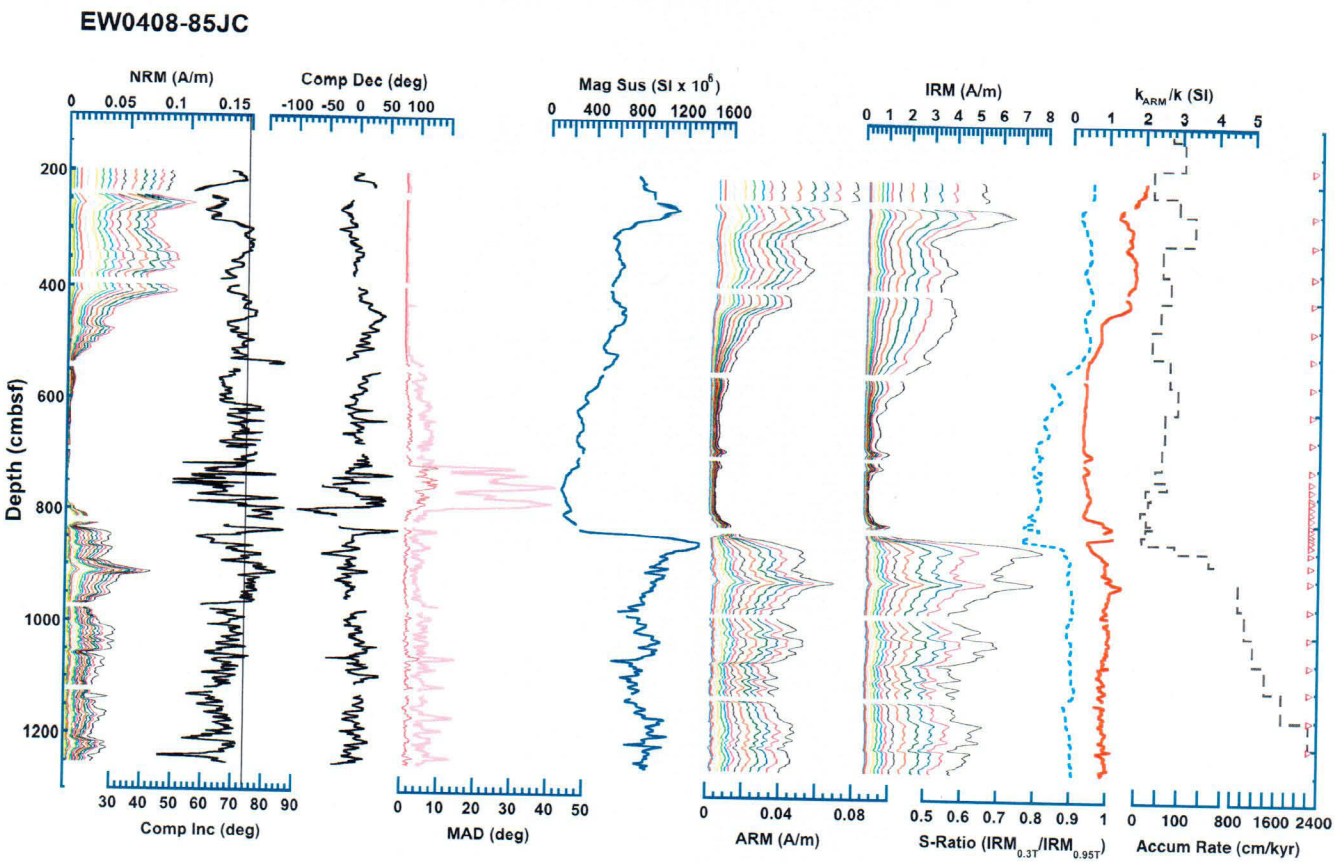

Fig. 5. Bulk magnetic parameters from EW0408-85JC. From left to right: natural remanent magnetization (NRM) intensities after AF-demagnetization at steps from 0–100 mT, optimized (as described in text; also see Fig. S.4) component inclinations (GAD = 74°, shown as dashed line), declinations, and maximum angular deviations (MAD) calculated from the 10–60 mT steps (pink from all steps, red from optimized steps only), magnetic susceptibility, anhysteretic remanent magnetization (ARM) and isothermal remanent magnetization (IRM) acquired at a 0.3 T DC field after AF-demagnetization at steps from 0–80 mT, S-Ratio, κ_{ARM}/κ, and sediment accumulation rates derived from the planktonic radiocarbon dates (red triangles). (For interpretation of the colors in this figure, the reader is referred to the web version of this article.)

between 550–1200 cmbsf (Fig. 4). S-ratios vary around 0.95 and κ_{ARM}/κ values vary around 1.4, implying a relatively consistent ferrimagnetic mineralogy of generally uniform average magnetic grain-size, estimated to be ~5 μm using the calibration of King et al. (1982). Ratios derived from hysteresis parameters (Fig. S.6) plot in the pseudo single domain (PSD) field (Day et al., 1977).

Core EW0408-85JC, in contrast to the shelf site, exhibits pronounced millennial-scale changes in magnetic properties, reflecting evolution of the depositional environment over the last 17,400 yrs (Fig. 5). NRM, ARM and IRM (after 30 mT AF demagnetization) have respective means of 0.018 ± 0.016 A/m, 0.015 ± 0.01 A/m and 0.95 ± 0.5 A/m (Fig. 5), showing greater variance, albeit over a much longer time interval, than observed at EW0408-79JC. Low remanence intensities observed between ~550–840 cmbsf contrast with higher intensities at the top and bottom of the core, resulting in the much greater long-term variability. The S-ratio and κ_{ARM}/κ follow a similar pattern, with lower values in the central part of the core, consistent with magnetic mineralogy and/or grain-size changes.

High magnetic intensities in EW0408-85JC are observed between the core top and 530 cmbsf (<7200 cal ybp) and below 800 cmbsf (>13,500 cal ybp). MAD values covary, with the upper ~530 cmbsf displaying well-defined magnetization with values mostly <1°. MAD values are higher and more variable below 530 cmbsf, though generally less than 10° except for the deglacial interval between 715–795 cmbsf (~10,100–12,700 cal ybp) that is characterized by much lower NRM intensities ($8 \times 10^{-4} \pm 6 \times 10^{-4}$ A/m at 30 mT AF demagnetization), 10–60 mT ChRM, MAD values approaching 40°, and component inclinations varying around a mean ~15° shallower than the GAD prediction for the site latitude.

For most of the EW0408-85JC record, the optimized component directions result in essentially identical results to those determined using all steps between 10–60 mT, though with (by definition) improved MAD values (Figs. S.45 and 5). The only significant differences occur in the lowest intensity interval, ~710–800 cmbsf, ~10,000 to 13,500 cal ybp, where MAD values are significantly reduced from as high as around 40° to <10° and the resultant directions show reduced variability and improved serial correlation with overall steeper and more GAD-like inclinations (Fig. S.4). The optimized ChRM directions are similar to those obtained from the 20 mT AF demagnetization step, suggesting that the optimized component directions largely reflect a low-coercivity primary magnetization appropriate for recording PSV.

3.5. Temperature dependent and infield magnetic measurements

Examination of magnetic hysteresis properties, thermal demagnetization behavior (Ms/T), and low-temperature remanence (RTLT-SIRM) curves allows further insights into the magnetic properties of EW0408-85JC (Fig. 6; Fig. S.7). Outside of the low intensity interval in 85JC (~710–850 cmbsf), ratios derived from the hysteresis parameters plot in the pseudo single domain (PSD) field of a Day et al. (1977) diagram (Fig. 6a), falling slightly above the theoretical magnetite SD to MD mixing line (Dunlop, 2002). In the low intensity interval, in contrast, hysteresis ratios are much more scattered with coercivity ratios much higher (Fig. 6a) than would be typically expected for the magnetite (e.g. Dunlop, 2002). Low S-ratios

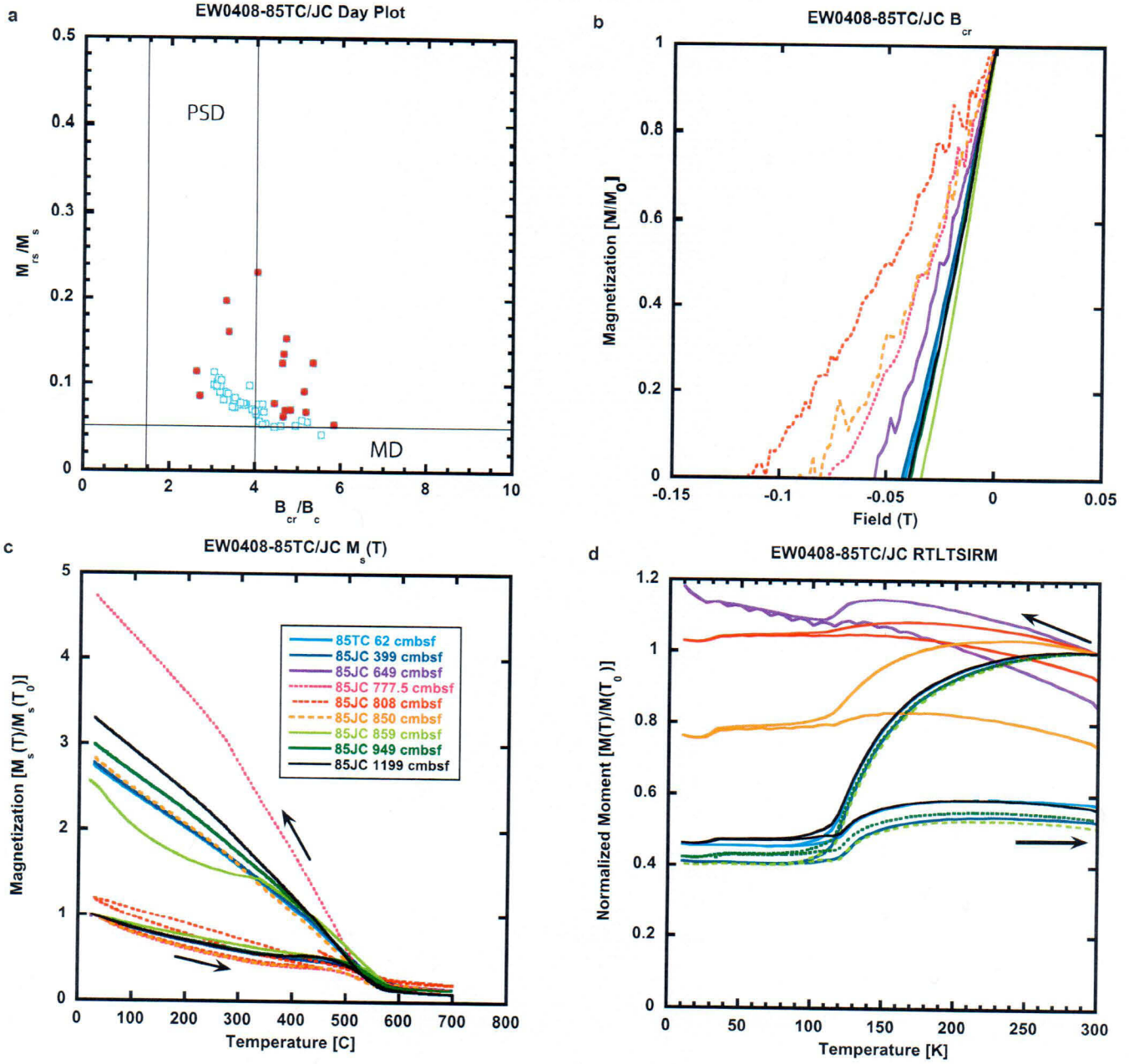

Fig. 6. Rock magnetic measurements on selected samples from EW0408-85JC including **a)** hysteresis ratios M_{rs}/M_s vs. B_{cr}/B_c presented in the form of a Day et al. (1977) diagram (samples from the weakly magnetized interval between 710–850 cmbsf denoted with solid red symbols), **b)** backfield experiments normalized to the magnetization at 0 T, **c)** thermal demagnetization curves normalized to remanence at room temperature (~22–25 °C) and **d)** low-temperature SIRM experiments normalized to remanence at starting temperature (300 K). Note that Ms/T data is unavailable for the sample from 649 cmbsf, and LTRTSIRM data is unavailable from 777.5 cmbsf. (For interpretation of the references to color in this figure, the reader is referred to the web version of this article.)

(<0.9) are also observed in this interval providing additional evidence for a greater proportion of high coercivity magnetic minerals (Fig. 5).

A more detailed examination of the rock magnetic properties was performed on nine samples spanning the range of sediment lithologies present in EW0408-85TC/JC: three from Holocene sediments (62, 399, and 649 cmbsf), two from the organic-rich material deposited during deglaciation (777.5 and 808 cmbsf), and four from the late glacial diamict (850, 859, 949, and 1199 cmbsf). All hysteresis loops (detrended to correct for the slope of the paramagnetic contribution) are broadly consistent with a magnetite mineralogy (Fig. S.7), although hysteresis loop widths from samples 777.5, 808, and 850 cmbsf are somewhat greater than for samples above (62 and 399 cmbsf) and below (859–1199 cmbsf), indicative of a high-coercivity contribution to remanence (e.g., hematite; Tauxe, 1998). The thermal demagnetization curves from all depths measured show a Curie point of ~580 °C, indicative of magnetite (Fig. 6c). A transient increase in magnetization starting at ~400 °C may indicate some contribution from Ti-poor titanomagnetite or titanomaghemite exolving to form magnetite (Özdemir and O'Reilly, 1981). The role of magnetite as a remanence carrier is supported by the RTLTSIRM curves, all of which display a transition at ~120 K (e.g., Verwey, 1939) (Fig. 6d) that is considered to be diagnostic of magnetite (e.g., Jackson et al., 2011). However, samples between 649 and 808 cmbsf (less 777.5 cmbsf, for which no data is available) have a weaker transition and a 'humped' ap-

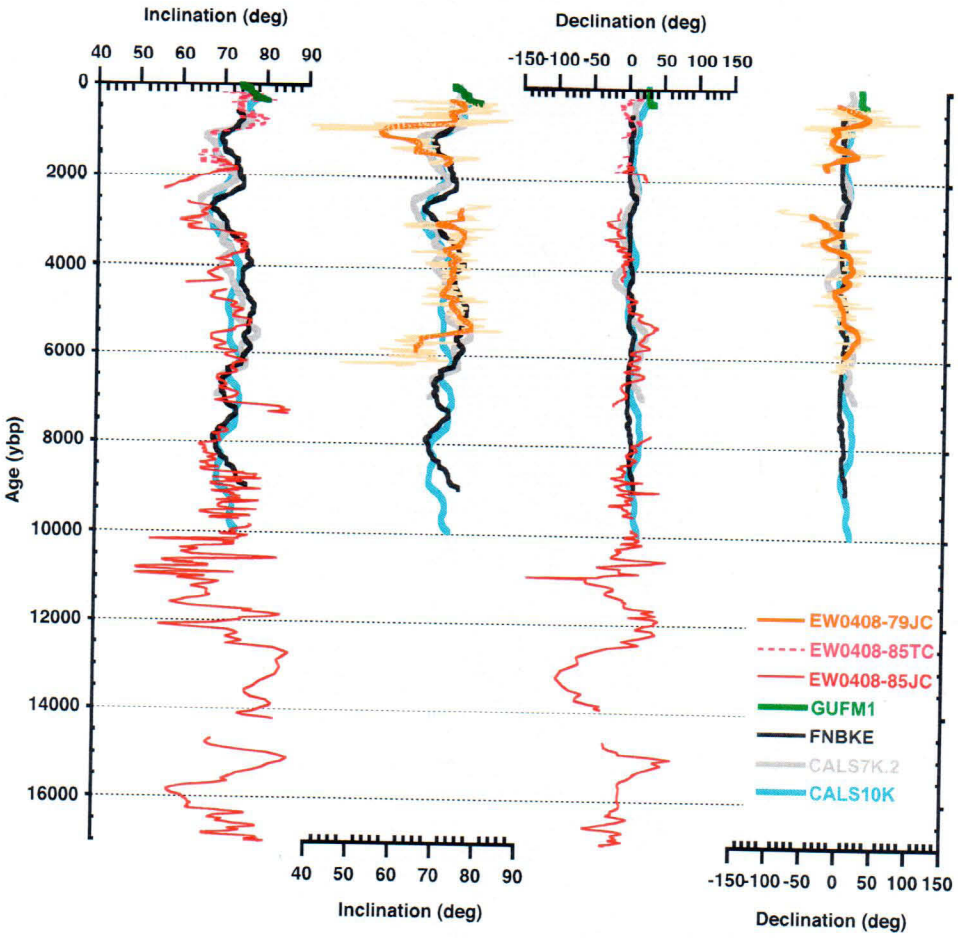

Fig. 7. Characteristic remanent magnetization inclinations and declinations from EW0408-85TC/JC (red/pink) and EW0408-79JC (orange; 100-yr smoothed record shown in bold), superimposed on the site predictions from the Holocene CALS10K.2 (light blue, Constable et al., 2016), FNBKE (dark gray, Nilsson et al., 2010) and historic GUFM1 (dark green, Jackson et al., 2000) field models. (For interpretation of the colors in this figure, the reader is referred to the web version of this article.)

pearance between 300 K and the ~120 K Verwey transition, likely related to the convolved presence of maghemite and magnetite (Özdemir and Dunlop, 2010). The presence of a high-coercivity remanence carrier in this interval is further supported by the backfield curves (Fig. 6b) and high B_{cr} values (Fig. S.8). These higher B_{cr} values observed for the deglacial (~710–850 cmbsf) interval persist in the post-heating B_{cr} curves, supporting an interpretation of hematite or maghemite surface oxidation of magnetite grains (e.g., Özdemir and Dunlop, 1996; Passier et al., 2001).

4. Discussion

4.1. Magnetic remanence carriers and geomagnetic recording fidelity

Although the preservation of physical structure in EW0408-79JC argues that sedimentation is episodic on short, perhaps annual, timescales (e.g., Jaeger and Nittrouer, 2006), the overall high sediment accumulation rate and general consistency in mud-dominated lithofacies implies that PSV features on centennial to millennial timescales should be preserved with little if any smoothing or temporal offset. With the exception of the massive sandy-silt interval excluded from interpretation (Fig. 4), ARM and IRM magnetizations, S-ratios and κ_{ARM}/κ values in EW0408-79JC all suggest the presence of a homogeneous population of low-coercivity magnetic remanence carriers (i.e. magnetite) through most of the last 6200 yrs.

The longer record in core EW0408-85JC displays a more complicated depositional and preservation history. A low-intensity interval between ~530–800 cmbsf (~7200–13,500 cal ybp; Fig. 5), indicates a change in magnetic mineralogy likely driven by the combined effects of changing sediment source, transport, and depositional regime along with early diagenesis (Karlin and Levi, 1983), the latter perhaps related to discrete episodes of deglacial benthic hypoxia previously documented at this site (Davies et al., 2011; Addison et al., 2012). S-ratios below 0.9 (Fig. 5) and elevated B_{cr} (Figs. S.7 and S.8) document a magnetic assemblage with a greater proportion of high-coercivity minerals (e.g., hematite, maghemite) corresponding to surface oxidation of magnetite particles over the 710–850 cmbsf interval. However, the presence of magnetite is clearly indicated by Curie temperature analyses, Verwey transitions (Fig. 6), as well as by magnetic hysteresis data (Fig. S.7), through the deglacial and early Holocene portions of the core. We thus infer that a primary (depositional or post-depositional) remanent magnetization is preserved with directions that can be interpreted as geomagnetic in origin throughout the EW0408-85JC record, though with less precision in the 710–850 cm (10,000–14,700 cal ybp) interval. Lithologic variability in excess of recommended criteria (Tauxe, 1993) make both EW0408-85JC and EW0408-79JC non-ideal candidates for relative paleointensity reconstructions.

4.2. Paleomagnetic secular variation

Fig. 7 shows the composite (trigger core/jumbo piston core) ChRM inclinations and declinations for the EW0408 sites on their independent age models compared with global field model predictions for the site location. Inclinations at both sites, smoothed

using a Gaussian filter with a 100-yr 1σ width to facilitate comparison, are generally consistent with historical (GUFM1; Jackson et al., 2000) and paleo (CALS10K.2; Constable et al., 2016; FNBKE; Nilsson et al., 2010, 2011) global field model predictions. Agreement between models and data suggest that PSV is recorded by these continental margin sediments and, in turn, that the models are capturing field dynamics in a region poorly constrained by prior data. Distinctions do exist; for example the almost 20° change from low to high inclination at ~950 cal ybp in EW0408-79JC is nearly twice the magnitude of global field model predictions. Unfortunately, part of this inclination event occurs within a core break at EW0408-85TC (Fig. S.3) and is thus not as well recovered, but it is consistent with a similar inclination event recorded in volcanic (Hagstrum and Champion, 2002) and archeomagnetic data (Hagstrum and Blinman, 2010) from the western US. In general the CALS10K.2 model predicts less variability than observed in either record, although there is considerable similarity on millennial timescales (Fig. 7).

The older part of the EW0408-85JC PSV record (>10,000 cal ybp) suggests larger amplitude millennial-scale variability than is observed in the Holocene, though it is conceivable that part of this variability could result from uncorrected diagenetic influence on the PSV record between ~10,000–14,700 cal ybp, as discussed in Section 4.1 and should be initially treated as suspect. Global field models provide no assistance during this time interval, however, the independently dated (via eight radiocarbon dates) Grandfather Lake, Alaska PSV record (Geiss and Banerjee, 2003) only 700 km WNW of the EW0408-85JC site, also preserves high amplitude inclination variations prior to 10,000 cal ybp (Fig. 8).

As with any sedimentary PSV record obtained via piston coring, declinations are less straightforward than inclinations. Several additional corrections were made after initially rotating the mean declination of the entire core to zero. The most significant was removal of a linear trend from EW0408-85TC, consistent with rotation during core penetration. The linear-corrected declination was then rotated to be consistent with historical GUFM model predictions (mean declination for the last 400 yrs is ~28°) to correct for the lack of azimuthal control (Fig. 7). EW0408-85JC declinations were then rotated to match the mean of the trigger core. Section 2 was rotated an additional 20° to account for misalignment during core splitting clearly visible on the core liner. The resulting declination time series from EW0408-85TC/JC and EW0408-79JC are similar, however agreement with the global paleo-field models is variable (Fig. 7) and additional records are needed for a robust evaluation of regional declination.

4.3. Regional PSV comparisons and generation of a NE Pacific stack

Negative inclination anomalies of much greater magnitude than have been observed historically, characterized by gradual growth and abrupt recovery, have been recognized in volcanic (Hagstrum and Champion, 2002) and archeomagnetic (Hagstrum and Blinman, 2010) PSV records from the western US. Similar features have been found in sediment PSV records from the central (Lund, 1996) and western US (Verosub et al., 1986). Building upon historical (Thompson and Barraclough, 1982) and paleomagnetic (Lund, 1996) observations, the apparent similarity of PSV in the western US (Verosub et al., 1986; Hagstrum and Champion, 2002; Hagstrum and Blinman, 2010) with sites in Alaska (Geiss and Banerjee, 2003), the Chukchi Sea (Lisé-Pronovost et al., 2009) and the Beaufort Sea (Barletta et al., 2010) implies that at least some aspects of the geomagnetic field behave coherently over roughly a continental scale (Lund, 1996). However the lack of strong independent chronologies for many of these records has remained the weakest point in this inference.

Stacking independently-dated regional records from different depositional environments helps to circumvent errors which accompany the recording, preservation, and recovery process at individual sites by enhancing shared patterns of variation. Any resulting coherence is likely to reflect regional geomagnetic history, with a quantifiable estimate of uncertainty. In addition to the EW0408-85TC/JC PSV record we include three continuous, independently-dated Pacific-sector paleomagnetic records of Holocene PSV in a stack: Lake Waiau, Hawaii Core 82-2 (19.8°N, 155.5°W; Peng and King, 1992), Fish Lake, Oregon (42.7°N, 118.7°W; Verosub et al., 1986), and Grandfather Lake, Alaska (59.8°, 158.6°W; Geiss and Banerjee, 2003). While we note EW0408-79JC and EW0408-85JC show consistent PSV behavior for their period of overlap, we elect to use only EW0408-85TC/JC in the generation of this NE Pacific Stack as this record is of similar resolution to the others and our focus is on longer-term variability and spatial coherence. Lake Waiau core 82-2 is evaluated on an updated age model using the published dates recalibrated to Intcal13 (Peng and King, 1992; Reimer et al., 2013). Fish Lake, Oregon (42.7°N, 118.7°W; Verosub et al., 1986), is presented on the adjusted chronology proposed by Hagstrum and Champion (2002) for the upper part of the record with an updated radiocarbon calibration to Intcal13, avoiding the mixed use of radiocarbon and tephra ages (Verosub et al., 1986) that complicates the application of modern calibrations in the early Holocene.

In order to evaluate the coherence of Holocene geomagnetic inclination records across ~40° in latitude, we subtract the GAD-predicted inclination for each site location from the inclination record, noting that in the case of Fish Lake, an inclination correction of ~5° has already been applied (Verosub et al., 1986). The resulting records of inclination deviation from GAD (ΔI) were then filtered with a Gaussian filter of 100-yr 1-σ width and interpolated to a constant resolution of 100 yrs on their independent chronologies through intervals for which data was collected, and an average ΔI value was calculated across all cores available for each time point (Fig. 8).

To generate a North Pacific PSV declination stack all records were initially rotated to a mean of 0, and relocated to the position of EW0408-85JC via dipole transformation to account for latitudinal effects on declination. Following this initial step, treatment was the same as for the inclination stack: each record was filtered with a Gaussian filter of 100-yr 1-σ width and interpolated to a constant 100-yr resolution on their independent chronologies, then averaged at each time step across all cores for which data was available (Fig. S.9). Grandfather Lake provides no declination data due to lack of azimuthal orientation of the 1-m Livingston core drives during core collection (Geiss and Banerjee, 2003). As a result, our declination stack includes only three regional North Pacific records. Of the remaining three records, Lake Waiau was collected using 1-m Livingston core drives, similar to Grandfather Lake, and Fish Lake was collected using non-oriented 3-m offset drives, both of which present challenges to and reduce confidence in reconstructions of declination. Therefore our primary focus will be on the inclination record.

Although the age models are of varying resolutions and accuracies, and the depositional environments are diverse and widely dispersed, a number of robustly defined, millennial-scale inclination anomalies (ΔI), both positive and negative, appear as coherent features captured in the NE Pacific sedimentary inclination anomaly stack (NEPSIAS). The three largest $-\Delta I$ anomalies are found in the late Holocene: two well-known $-\Delta I$ events from regional records at ~1400, and ~3000 (e.g., Hagstrum and Champion, 2002; Herrero-Bervera and Valet, 2007; Hagstrum and Blinman, 2010), and a third at ~4500 cal ybp (Fig. 8). Considering NRM acquisition and stacking-induced smoothing, the amplitude and rates of change of these ΔI features within NEPSIAS are likely

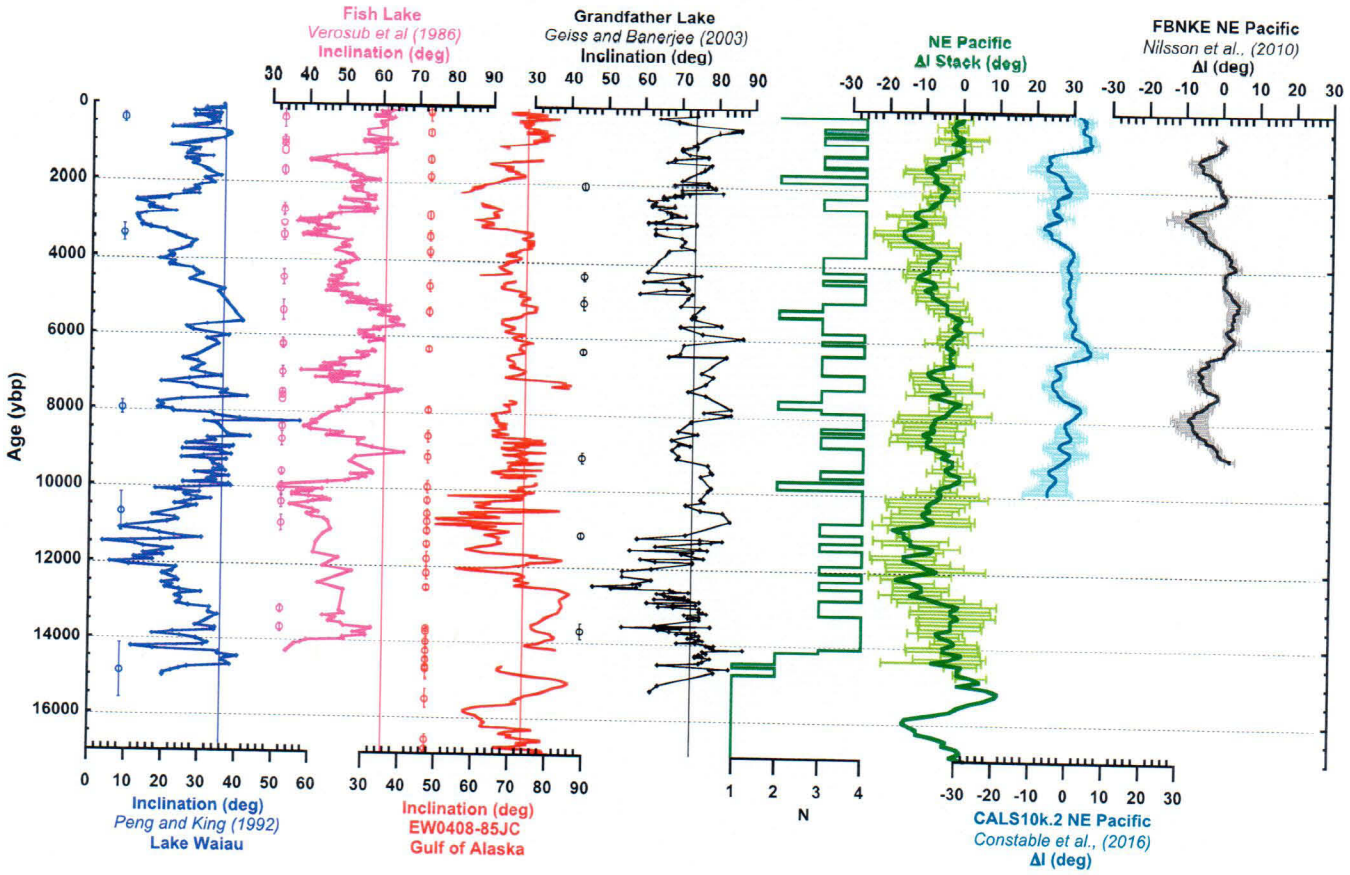

Fig. 8. Northeast Pacific Holocene inclination records, compared on independent chronologies. From left to right: Lake Waiau, Hawaii (solid purple line, Peng and King, 1992), Fish Lake, Oregon (solid pink line, Verosub et al., 1986), Gulf of Alaska record EW0408-85TC/JC (dashed/solid red line), and Grandfather Lake, Alaska (hollow black diamonds, Geiss and Banerjee, 2003). GAD inclination values are shown as a solid line for each record, and the calibrated radiocarbon dates that provide chronological control for each record are shown as discrete symbols with 1-σ error. A NE Pacific inclination anomaly stack (NEPSIAS) (shown in green) was generated by adjusting each record to deviation from its GAD value (ΔI) following interpolation to 100-yr resolution and smoothing with a 100-yr Gaussian filter. The number of records (N) available for each time step is shown to the left of the stack. Stacks generated from inclination predictions for the same four sites from CALS10K.2 (light blue, Constable et al., 2016), and FNBKE (dark gray, Nilsson et al., 2010) are also shown. Uncertainty envelopes reflect standard error. (For interpretation of the colors in this figure, the reader is referred to the web version of this article.)

minimum estimates, although they are somewhat larger than ΔI features in global field model stacks generated from CALS10k.2 and FNBKE predictions for the NEPSIAS sites (Fig. 8). Additional $-\Delta I$ anomalies are observed in the early to mid-Holocene, centered at ~7000 and ~8500 cal ybp; while the modeled stacks capture shallow inclination features at similar times, there are differences which highlight the need for additional records and/or re-evaluation of model predictions for Pacific PSV. NEPSIAS extends beyond the limit of global field models, capturing an additional broad $-\Delta I$ anomaly centered around 11,500 cal ybp, with EW0408-85JC suggesting another large $-\Delta I$ anomaly at ~16,000 cal ybp. (Fig. 8).

4.4. Drivers of Northern Hemisphere paleomagnetic secular variation

Deviations from GAD similar to those in NEPSIAS have been observed at similar times in high-resolution North Atlantic PSV records (Stoner et al., 2013). In the northern North Atlantic (NNA) these deviations are primarily expressed as large eastward shifts in declination associated with highs in European/Mediterranean archeomagnetic intensity over the last ~8000 cal ybp (Genevey et al., 2008). NEPSIAS builds upon these observations by showing that $-\Delta I$ anomalies in the NE Pacific are roughly synchronous with eastward NNA declinations over the full 11,500 yr length of the NNA record (Stoner et al., 2013) (Fig. 9).

The overall morphologies of the NEPSIAS and NNA declination records are similar, with no statistically apparent lead or lag between NEPSIAS $-\Delta I$ anomalies and NNA declination (Fig. S.10). Archeomagnetic (Hagstrum and Blinman, 2010) and lava-based (Hagstrum and Champion, 2002) inclination reconstructions are also temporally consistent with NEPSIAS and NNA declination (Fig. 9) supporting the ability of the stack to reduce errors associated with the sediment magnetization acquisition process and/or systematic dating uncertainties. Steeper NEPSIAS inclinations are associated with westward NNA declination shifts and, for the last ~3000 cal ybp, higher North American intensities (e.g., Genevey et al., 2008); although little North American intensity data is available beyond 3000 cal ybp, the relationship between NEPSIAS inclination and NNA declination appears to hold through the last 11,500 cal ybp (Figs. 9 and S.10).

Well-resolved PSV reconstructions spanning the last 5,000 yrs indicate that field morphology can be roughly broken into two modes consistent with a geomagnetic flux lobe over North America alternating in dominance with a flux lobe over Europe (Gallet et al., 2009; Stoner et al., 2013). The 'North American mode', characterized by relatively steep inclinations and high intensities in N. America, westward declinations in the N. Atlantic, and low intensities in Europe, is conceptually consistent with the time-averaged historical field of the past few centuries (Fig. 1; Jackson et al., 2000). The alternate 'European mode' is characterized by periods of shallow inclination and low intensity in N. America,

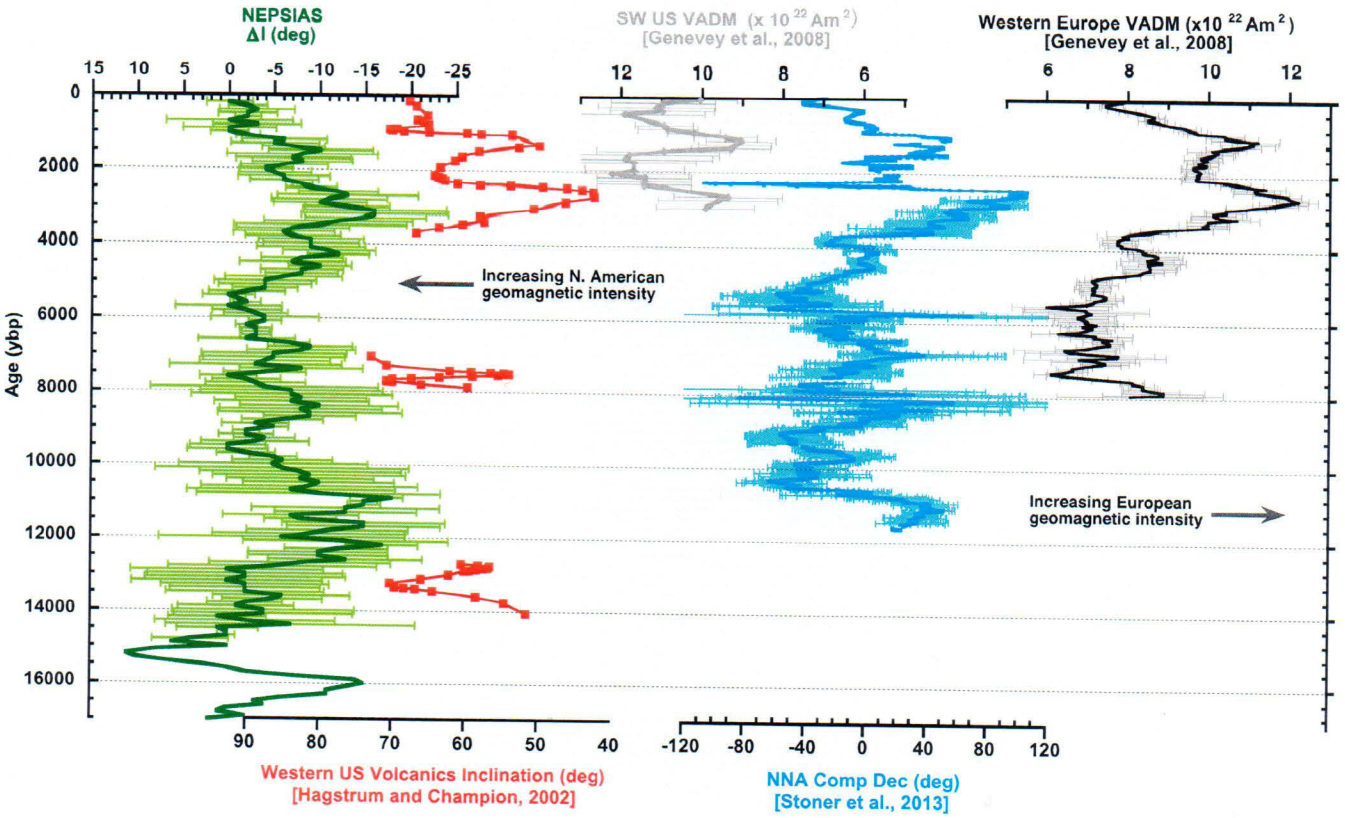

Fig. 9. NE Pacific inclination anomaly stack (NEPSIAS) compared with (from left to right) archeomagnetic inclinations from Western US volcanics (red; Hagstrum and Champion, 2002), archeomagnetic North American virtual axial dipole moments (VADM) (gray; Genevey et al., 2008), Northern North Atlantic (NNA) declination as determined via composite records from Greenland and Iceland (blue; Stoner et al., 2013), and Western European VADM (black; Genevey et al., 2008). Note axis reversed on NEPSIAS relative to Fig. 8 for ease of comparison. Uncertainty envelopes reflect standard error. (For interpretation of the colors in this figure, the reader is referred to the web version of this article.)

eastward declinations in the N. Atlantic, and high intensities in Europe, consistent with the time-averaged mid-to-late Holocene field (Amit et al., 2011). Inflection points for either steep NEPSIAS inclinations and westward NNA declinations, or shallow NEPSIAS inclination and eastward NNA declination, coincide with archeomagnetic jerks defined by Gallet et al. (2003) over the last ~3000 cal ybp. Based on this relationship, changes in NEPSIAS inclination may predict archeomagnetic jerks and/or periods of enhanced dipole eccentricity (Gallet et al., 2009) beyond the temporal limit of archeomagnetic data.

Observations of coherent inclination changes across a vast, though as yet poorly-defined, area in the NE Pacific are generally consistent with the idea of a regional 'dipole window' (Cox, 1962), and the concept of subdued secular variation in the Pacific that has a long history. Secular variation in the Pacific nonetheless appears to co-vary with that in the dynamic Atlantic, suggesting that the Pacific is sensitive to temporal variability in the relative strength of distal flux-lobe features in quasi-persistent locations under North America and Europe.

5. Summary and conclusions

High-resolution sedimentary records from two cores on the Gulf of Alaska margin allow development of a ~17,400 yr record of regional geomagnetic variability. General agreement between the records on their independent chronologies confirms that local PSV is recorded, demonstrating that such archives, notwithstanding complexities due to variable sedimentary regimes, deposition rates, and diagenetic conditions, provide meaningful information on the past changes of the geomagnetic field. Much, but not all, of the observed directional variability is consistent with spherical harmonic (CALS10K.2; Constable et al., 2016) and/or VGP (FNBKE; Nilsson et al., 2010) predictions, suggesting that PSV in this region is governed by large-scale geomagnetic dynamics. Comparisons with other independently-dated sedimentary paleomagnetic records from the greater NE Pacific region (Verosub et al., 1986; Peng and King, 1992; Geiss and Banerjee, 2003) indicate largely coherent inclination records that we combine to produce a NE Pacific sedimentary inclination stack (NEPSIAS). This stack documents a common signal over a >30° longitude and latitude region spanning from Alaska through Oregon to Hawaii (Fig. 8).

Comparison of NEPSIAS with high quality declination records from the northern North Atlantic shows NEPSIAS negative ΔI anomalies are associated with eastward NNA declination and NEPSIAS positive ΔI anomalies are associated with westward NNA declinations (Fig. 9). Comparison with regional geomagnetic intensity, over the past ~3000 yrs in the North America and back nearly 8000 yrs in the Euro/Mediterranean region (e.g., Genevey et al., 2008) suggest these directional records reflect variability in the relative strength of the North American flux lobe and Euro/Mediterranean flux lobe (Gallet et al., 2009; Stoner et al., 2013). Persistence of these features implicates a long-lived organizing structure imposed on the geomagnetic field, perhaps by the lower mantle (Bloxham and Gubbins, 1987), that profoundly influences the spatial and temporal patterns of PSV. Although additional continuous and independently dated records are required to assess the spatial and temporal scales over which these geomagnetic structures persist, this study highlights a straightforward relationship between North Atlantic and North Pacific PSV and supports the correlation of centennial to millennial-scale geomagnetic variability as

a long distance chronostratigraphic tool throughout the Holocene and perhaps beyond.

Acknowledgements

The authors gratefully acknowledge the crew and science party of R/V Maurice Ewing cruise EW0408, the staff of the OSU Marine Geology Repository, the OSU CEOAS Stable Isotope laboratory, the UC Irvine Keck AMS laboratories, and the University of Minnesota Institute of Rock Magnetism (which also provided a visiting fellowship for collection of rock magnetic data from EW0408-85JC). We also thank Bernie Housen, Elizabeth Patterson, and Robert Hatfield for facilitating and collecting additional hysteresis data at Western Washington University. This work was supported by NSF grants EAR-0711584 (JSS, ACM) EAR-1215888 (JSS), OCE-0351043 (Jaeger).

Appendix A. Supplementary material

Supplementary material related to this article can be found online at http://dx.doi.org/10.1016/j.epsl.2017.05.022. These data include the Google map of the most important areas described in this article.

References

Addison, J.A., Finney, B.P., Dean, W.E., Davies, M.H., Mix, A.M., Jaeger, J.M., 2012. Productivity maxima and sedimentary $\delta^{15}N$ during the Last Glacial Maximum termination in the Gulf of Alaska. Paleoceanography 27 (1). http://dx.doi.org/10.1029/2011/PA002161.

Amit, H., Korte, M., Aubert, J., Hulot, G., 2011. The time-dependence of intense archeomagnetic flux patches. J. Geophys. Res. 116, B12106.

Barletta, F., St-Onge, G., Stoner, J.S., Lajeunesse, P., Locat, J., 2010. A high-resolution Holocene paleomagnetic secular variation and relative paleointensity stack from eastern Canada. Earth Planet. Sci. Lett. 298, 162–174.

Bloemendal, J., King, J.W., Hall, F.R., Doh, S.J., 1992. Rock magnetism of Late Neogene and Pleistocene deep-sea sediments: relationship to sediment source, diagenetic processes, and sediment lithology. J. Geophys. Res. 97, 4361–4375.

Bloxham, J., Gubbins, D., 1987. Thermal core–mantle interactions. Nature 325, 511–513.

Constable, C., Korte, M., Panovska, S., 2016. Persistent high paleosecular variation activity in the Southern hemisphere for at least 10,000 years. Earth Planet. Sci. Lett. 453, 78–86.

Cowan, E.A., Brachfeld, S.A., Powell, R.D., Schoolfield, S.C., 2006. Terrane-specific rock magnetic characteristics preserved in glacimarine sediment from southern coastal Alaska. Can. J. Earth Sci. 43, 1269–1282.

Cox, A., 1962. Analysis of the present geomagnetic field for comparison with paleomagnetic results. J. Geomagn. Geoelectr. 13, 35–51.

Davies, M.H., Mix, A.C., Stoner, J.S., Addison, J.A., Jaeger, J., Finney, B., Wiest, J., 2011. The deglacial transition on the Southeastern Alaska Margin: meltwater input, sealevel rise, marine productivity, and sedimentary anoxia. Paleoceanography. http://dx.doi.org/10.1029/2010PA002051.

Davies-Walczak, M.H., Mix, A.C., Stoner, J.S., Southon, J., 2014. The flooding of Beringia and the onset of North Pacific Intermediate Water formation. Earth Planet. Sci. Lett. 397, 57–66.

Day, R., Fuller, M., Schmidt, V.A., 1977. Hysteresis properties of titanomagnetites: grain size and composition dependence. Phys. Earth Planet. Inter. 13, 260–267.

Dunlop, D.J., 2002. Theory and application of the day plot (M_{rs}/M_s versus H_{cr}/H_c) 1. Theoretical curves and tests using titanomagnetite data. J. Geophys. Res. 107, 2056.

Gallet, Y., Genevey, A., Courtillot, V., 2003. On the possible occurrence of "archaeomagnetic jerks" in the geomagnetic field over the past three millennia. Earth Planet. Sci. Lett. 214, 237–242.

Gallet, Y., Hulot, G., Chulliat, A., Genevey, A., 2009. Geomagnetic field hemispheric asymmetry and archeomagnetic jerks. Earth Planet. Sci. Lett. 284, 179–186.

Geiss, C.E., Banerjee, S.K., 2003. A Holocene–Late Pleistocene geomagnetic inclination record from Grandfather lake, SW Alaska. Geophys. J. Int. 153, 497–507.

Genevey, A.Y. Gallet, Constable, C.G., Korte, M., Hulot, G., 2008. ArcheoInt: an upgraded compilation of geomagnetic field intensity data for the past ten millennia and its application to the recovery of the past dipole moment. Geochem. Geophys. Geosyst., http://dx.doi.org/10.1029/2007GC001881.

Hagstrum, J.T., Champion, D.E., 2002. A Holocene paleosecular variation record from 14C-dated volcanic rocks in western North America. J. Geophys. Res. 107 (B1). http://dx.doi.org/10.1029/2001JB000524.

Hagstrum, J.T., Blinman, E., 2010. Archeomagnetic dating in western North America: an updated reference curve based on paleomagnetic and archeomagnetic data sets. Geochem. Geophys. Geosyst. 11, Q06009. http://dx.doi.org/10.1029/2009/GC002979.

Haslett, J., Parnell, A., 2008. A simple monotone process with application to radiocarbon-dated depth chronologies. J. R. Stat. Soc., Ser. C. Appl. Stat. 57 (4). 399–418.

Herrero-Bervera, H., Valet, J-P., 2007. Holocene paleosecular variation from dated lava flows on Maui (Hawaii). Phys. Earth Planet. Inter. 161, 267–280.

Jackson, A., Jonkers, A.R.T., Walker, M.R., 2000. Four centuries of geomagnetic secular variation from historical records. Philos. Trans. R. Soc. Lond. A, Math. Phys. Eng. Sci. 358, 957–990.

Jackson, M., Moskowitz, B.M., Bowles, J., 2011. Interpretation of low-temperature data part III: the magnetite Verwey transition (part a). IRM Q. (ISSN 2152-1972) 20 (4), 1–11.

Jaeger, J.M., Nittrouer, C.A., 2006. A quantitative examination of modern sedimentary lithofacies formation on the glacially influenced Gulf of Alaska continental shelf. Cont. Shelf Res. 26, 2178–2204.

Karlin, R., Levi, S., 1983. Diagenesis of magnetic minerals in recent haemipelagic sediments. Nature 303, 327–330.

King, J., Banerjee, S.K., Marvin, J., Ozdemir, O., 1982. A comparison of different magnetic methods for determining the relative grain size of magnetite in natural materials: some results from lake sediments. Earth Planet. Sci. Lett. 59, 404–419.

Kirschvink, J.L., 1980. The least-squares line and plane and the analysis of palaeomagnetic data. Geophys. J. R. Astron. Soc. 62, 699–718.

Lisé-Pronovost, A., St-Onge, G., Brachfeld, S., Barletta, F., Darby, D., 2009. Paleomagnetic constraints on the Holocene stratigraphy of the Arctic Alaskan margin. Glob. Planet. Change 68, 85–99.

Lund, S.P., 1996. A comparison of Holocene paleomagnetic secular variation records from North America. J. Geophys. Res. 101, 8007–8024.

Merrill, R., McElhinny, M., McFadden, P., 1996. The Magnetic Field of the Earth. Academic Press, San Diego, CA, 531 pp.

Nilsson, A., Snowball, I., Muscheler, R., Bertacchi Uvo, C., 2010. Holocene geocentric dipole tile model constrained by sedimentary paleomagnetic data. Geochem. Geophys. Geosyst. 11. http://dx.doi.org/10.1029/2010GC003118.

Nilsson, A., Muscheler, R., Snowball, I., 2011. Millennial scale cyclicity in the geodynamo inferred from a dipole tilt reconstruction. Earth Planet. Sci. Lett. 311 (3), 299–305.

Nilsson, A., Holme, R., Korte, M., Suttie, N., Hill, M., 2014. Reconstructing Holocene geomagnetic field variation: new methods, models, and implications (2014). Geophys. J. Int.. http://dx.doi.org/10.1093/gji/ggu120.

Özdemir, Ö., Dunlop, D.J., 1996. Thermoremanence and Neel temperature of goethite. Geophys. Res. Lett. 23, 921–924.

Özdemir, Ö., Dunlop, D.J., 2010. Hallmarks of maghemitization in low-temperature cycling of partially oxidized magnetite nanoparticles. Geophys. Res. Lett. 114. http://dx.doi.org/10.1029/2009JB006756.

Özdemir, Ö., O'Reilly, W., 1981. High temperature hysteresis and other magnetic properties of synthetic monodomain titanomagnetites. Phys. Earth Planet. Inter. 25, 406–418.

Passier, H.F., deLange, G.J., Dekkers, M.J., 2001. Magnetic properties and geochemistry of the active oxidation front and the youngest sapropel in the eastern Mediterranean Sea. Geophys. J. Int. 145, 604–614.

Peng, L., King, J.W., 1992. A late Quaternary geomagnetic secular variation record from Lake Waiau, Hawaii, and the question of the Pacific nondipole low. J. Geophys. Res. 97 (B2), 4407–4424.

Praetorius, S.K., Mix, A.C., Jensen, B., Froese, D., Milne, G., Wolhowe, M.D., Addison, J.A., Prahl, F.G., 2016. Interaction between volcanism, isostatic rebound, and climate in Southeast Alaska during the last deglaciation. Earth Planet. Sci. Lett. 452, 79–89.

Reimer, P.J., Bard, E., Bayliss, A., Beck, J.W., Blackwell, P.G., Ramsey, C.B., Buck, C.E., Cheng, H., Edwards, R.L., Friedrich, M., Grootes, P.M., Guilderson, T.P., Haflidason, H., Hajdas, I., Hatte, C., Heaton, T.J., Hoffman, D.L., Hogg, A.G., Hughen, K.A., Kaiser, K.F., Kromer, B., Manning, S.W., Niu, M., Reimer, R.W., Richards, D.A., Scott, E.M., Southon, J.R., Staff, R.A., Turney, C.S.M., van der Plicht, J., 2013. Intcal13 and Marine13 radiocarbon age calibration curves 0–50,000 years cal BP. Radiocarbon 55, 1869–1887.

Roberts, A.P., Chang, L., Heslop, D., Florindo, F., Larrasoana, J.C., 2012. Searching for single domain magnetite in the 'pseudo-single-domain' sedimentary haystack: implications of biogenic magnetite preservation for sediment magnetism and relative paleointensity determinations. J. Geophys. Res.. http://dx.doi.org/10.1029/2012JB009412.

Stoner, J.S., Channell, J.E.T., Mazaud, A., Xuan, C., Strano, S.E., 2013. The influence of high latitude flux lobes on the Holocene paleomagnetic record of IODP Site U1305 and the northern North Atlantic. Geochem. Geophys. Geosyst. 14, 4623–4646. http://dx.doi.org/10.1002/ggge.20272.

Tarduno, J.A., Wilkinson, S.L., 1996. Non-steady state magnetic mineral reduction, chemical lock-in, and delayed remanence acquisition in pelagic sediments. Earth Planet. Sci. Lett. 144, 315–326.

Tauxe, L., 1993. Sedimentary records of relative paleointensity of the geomagnetic field: theory and practice. Rev. Geophys. 31, 319–354.

Tauxe, L., 1998. Paleomagnetic Principles and Practice. Kluwer Academic Publishers, Dordrecht, the Netherlands.

Thompson, R., Barraclough, D.R., 1982. Geomagnetic secular variation based on spherical harmonic and cross validation analyses of historical and archaeomagnetic data. J. Geomagn. Geoelectr. 34, 245–263.

Verosub, K.L., Mehringer Jr. P.J., Waterstraat, P., 1986. Holocene secular variation in western North America: paleomagnetic record from Fish Lake, Harney County, Oregon. J. Geophys. Res. 91, 3609–3623.

Verwey, E.J., 1939. Electronic conduction of magnetite (Fe_3O_4) and its transition point at low temperature. Nature 144, 327–328.